Am J Cancer Res 2023;13(6):2504-2516
www.ajcr.us /ISSN:2156-6976/ajcr0150191

Original Article

Multifunctional hybrid hydrogel for the prevention of post-surgery tumor recurrence

Teona Paresishvili, Merab Janelidze, Zurab Kakabadze

Department of Clinical Anatomy, Tbilisi State Medical University, Tbilisi 0186, Georgia

Received March 17, 2023; Accepted May 11, 2023; Epub June 15, 2023; Published June 30, 2023

Abstract: In this study, we present a multifunctional hybrid hydrogel (MFHH) for the prevention of postoperative tumor recurrence. MFHH consists of two components; component A - containing a gelatin-based cisplatin, which destroys the residual cancer after surgery, and component B - containing macroporous gelatin microcarriers (CultiSpher) loaded with freeze-dried bone marrow stem cells (BMSCs), which activates the wound healing process. We also evaluated the effects of MFHH in a subcutaneous Ehrlich tumor mouse model. MFHH acted as a local delivery system by directly supplying cisplatin to the tumor environment, resulting in excellent anti-cancer effects and minimal side effects. MFHH released cisplatin gradually to destroy the residual tumors, thereby preventing loco-regional recurrence. We have also demonstrated that BMSCs are able to inhibit residual tumor growth. Moreover, CultiSpher loaded with BMSCs acted as an injection 3D scaffold and easily filled the wound defect formed by tumor removal, and the paracrine factors of the freeze-dried BMSCs accelerated the wound healing process. The components of the MFHH can be used both separately and together. However, for the successful application of MFHH in clinical practice, it is necessary to study in more detail the role of paracrine factors of freeze-dried BMSCs in the inhibition or proliferation of residual cancer. These questions will be the focus of our future research.

Keywords: Multifunctional hybrid hydrogel, local drug delivery systems, cisplatin mechanism of action, macroporous gelatin microcarriers (CultiSpher), Ehrlich solid tumor, bone marrow stem cells

Introduction

Currently, surgery, chemotherapy, radiation therapy, immunotherapy, targeted therapy, and their combinations are widely used to treat cancer. Surgery is the major treatment option for various cancer types. However, despite radical tumor resection, loco-regional recurrence is often observed after surgery, which may be associated with residual cancer [1]. Surgical margins also are associated with the risk of local recurrence [2]. Frozen sections are the standard method for determining the resection margins [3]. Magnetic resonance and nuclear, micro-computed, positron emission, and photoacoustic tomography are used for intraoperative determination of residual tumor sizes [4-7]. Intraoperative near-infrared fluorescent imaging and intraoperative flow cytometry have also been proposed to detect residual tumor cells [8, 9]. Despite all the available detection and treatment methods, the incidence of loco-regional tumor recurrence remains high in patients with cancer. For example, local recurrence is observed in 67% of patients after glioblastoma surgery [10]. Local recurrence is also observed in 71.8% of patients after radical resection of pancreatic cancer [11]. Moreover, local and hepatic recurrences were observed in 71.8 and 61.5% of patients, respectively, after resection of pancreatic ductal adenocarcinoma, both accounting for 97% of the total recurrence rate [12]. Local recurrence also occurs in 51.5% of patients after resection of distal cholangiocarcinoma [13-15]. Postoperative radiation therapy, chemotherapy, or a combination of both is recommended to prevent recurrence after radical resection of the tumor. Although these methods significantly reduce the incidence of local relapses, their use is associated with the risk of side effects [16-20]. In recent years, intratumoral cisplatin/epinephrine-injectable gel and Cisplatin gel have been used for the treatment of liver cancer, gastric cancer and others [21-25]. Our attention was attracted to the gelatin-based hydrogels because they

are highly soluble in water and can easily bind to drug molecules [26]. In addition, gelatin is able to form polymeric vesicles or micelles through self-assembly and drug release [27]. Reports on exploiting gelatin nanocarriers in the pulmonary delivery of methotrexate for lung cancer therapy have also been made [28]. The authors have noted that gelatin has many advantages that allow it to be used for delivering anticancer drugs to the lungs. Redox- and MMP-2-sensitive drug delivery nanoparticles based on gelatin and albumin have been used for tumor-targeted delivery of paclitaxel [29]. Bovine serum albumin as a targeting ligand, and gelatin as a hydrophilic carrier and MMP-2 sensitive reagent were used for constructing the nanoparticles. In another study, spatial controlled multistage nanocarriers that are created through hybridization of dendrimers and gelatin nanoparticles for deep penetration and therapy into tumor tissue are also presented [30]. The authors have noted that in response to the high matrix metalloproteinase-2 (MMP-2) enzymes in the tumor microenvironment, multistage nanocarrier releases polyamidoamine (PAMAM) dendrimers and furtherly transports them into tumor cells. Collagen-hydroxyapatite [31], alginic acid [32], hyaluronic acid [33], PLA or PGA copolymers [34], Nucleoside-lipid [35], and others are currently used as carriers for the sustained release of cisplatin. Each of these carriers has its own advantages and disadvantages. However, most drug carriers have poor biodegradability, low bioavailability, inadequate tissue distribution, and potential toxicity, especially with long-term administration [36].

In this study, we present a multifunctional hybrid hydrogel (MFHH) for the prevention of postoperative tumor recurrence. MFHH consists of two components; component A - containing a gelatin-based cisplatin, which destroys the residual cancer after surgery, and component B - containing macroporous gelatin microcarriers (CultiSpher) loaded with freeze-dried BMSCs.

Material and methods

Tumor cells

Tumor cells were obtained from host mice with Ehrlich ascites carcinoma. First, ascitic fluid was aspirated by puncturing the abdominal cavity, cells were washed with phosphate-buffered saline (pH 7.4), and centrifuged at 200×*g* for 10 min. Cell viability was determined after trypan blue staining in a Neubauer chamber. Tumor cells were also stained with Giemsa.

Animals

Seventy outbred white male mice (six or eight-week-old) were purchased from the vivarium of Tbilisi State Medical University (Tbilisi, Georgia). Animals were kept 10 per cage under 12/12 h day/night cycles and provided pelleted rodent diet and water ad libitum. Six laboratory Lewis rats (eight-week-old; approximately 250 g) were used as donors to obtain the bone marrow stem cells (BMSCs).

All experimental procedures were performed in accordance with the EU Directive 2010/63/EU for animal experiments and the guidelines of the Animal Care and Use Committee of Tbilisi State Medical University.

Study design

All animals were divided into seven groups. After one week of acclimatization, mice of six groups were subcutaneously injected with 2.5×10^6 tumor cells in the dorsal region. Animals of the seventh group served as controls, which received a subcutaneous injection of saline into the dorsal region.

The treatment of animals was initiated 20 days from the injection when the tumor volume reached 200 ± 8 mm^3: Group I - tumor model (TM) + resection of 90% of the tumor (TR) + MFHH; Group II - TM + TR + gelatin hydrogel incorporating cisplatin (GHC); Group III - TM + TR + Cultispher loaded with BMSCs (CS-BMSCs) which filled the wound and covered the residual tumor tissue that remained after tumor resection; Group IV - TM + TR + BMSCs. The freeze-dried BMSCs were hydrated in 0.9% NaCl solution for 30 minutes. Afterwards, single injections of 5×10^5 BMSCs were made into the tail vein of the animals with a 30G; Group V - TM + TR; Group VI - TM + observation of animals without any treatment; Group VII - control group. Animals were injected with physiological saline subcutaneously in the dorsal region.

Surgical procedures were performed under anesthesia via intraperitoneal injections of ketamine (100 mg/kg) and xylazine (7 mg/kg).

Fabrication of MFHH

MFHH comprises two components, A and B. Component A was used to eliminate minimal residual cancer after surgery, and component B was used to activate the wound-healing process.

Fabrication of component A: Component A represents gelatin hydrogels incorporating cisplatin. To fabricate component A, we used the method proposed by Suzuki T, et al. (2022) [37]. Briefly, 1 g of commercially purchased gelatin was placed in 10 mL of distilled water at room temperature for 30 min and dissolved for 1 h at 40°C. To the dissolved gelatin solution, 30 mL of aqueous cisplatin solution (3 mg/mL) was added under constant magnetic stirring at room temperature for 1 h. Cisplatin was also used as a cross-linking agent for gelatin. The mixed aqueous solution was poured into a Dynalon polystyrene container (Spectrum) and kept at 4°C for 24 h. The resulting hydrogel was passed through fine test sieves with a pore size of 150 μm (Sigma Aldrich). Ethanol was used to dehydrate the granules. The granules were degassed in a desiccator for 10 h to remove ethanol. According to the method of O'Connell et al. (2019), sterilization was carried out with ethylene oxide in an Anprolene EtO sterilizer (Anderson Sterilizers Inc., USA) at room temperature (23°C) for a 12/12 h day/night cycle, followed by a 12-h purge to wash off the remaining ethylene oxide [38]. Cisplatin gel was stored under sterile conditions at -20°C until use.

Fabrication of component B: Component B is an injectable 3D scaffold consisting of macroporous gelatin microcarriers (CultiSpher) loaded with freeze-dried rat BMSCs and a fibrinogen gel with thrombin.

Isolation of rat BMSCs and subsequent loading on CultiSpher

BMSCs were isolated via density gradient centrifugation at 400×*g* for 30 min at room temperature using Ficoll Paque Plus (GE Healthcare Bio-Sciences, Pittsburgh, PA, USA), as previously described [39]. Then, 0.3 g rehydrated CultiSpher and rat BMSCs (7.0×10^6) were placed in a 24-well Companion Plate (Falcon; Corning Life Sciences) and incubated at 37°C with 5% CO_2 and 90% humidity. Dulbecco's modified Eagle's medium containing 10% fetal bovine serum (Millipore Sigma), 50 U/mL penicillin, and 0.05 mg/mL streptomycin was used as the cell culture medium. BMSCs were co-cultured with CultiSpher for seven days and the culture medium was changed every three days. After culture, CultiSpher loaded with stem cells was freeze-dried with a lyophilizer (Heto Power Dry PL6000 Freeze Dryer; Sjia Lab, Shenzhen, China).

To construct the fibrinogen gel, we used the protocol of Yuan et al. (2011) [40], with modifications. Briefly, the original solution of fibrinogen with a concentration of 33 mg/mL was placed in 20 mM HEPES buffer in 0.9% saline and slowly mixed for 3 h at 37°C. Next, 0.1 g of rehydrated CultiSpher, which was loaded with freeze-dried BMSCs, was placed into the fibrinogen gel. Then, the fibrinogen solution together with CultiSpher was poured into aliquots of 1 mL and stored at -20°C until use.

Thrombin solution was prepared by adding 18 mL of 0.9% saline and 2 mL of sterile deionized water to 500 U of thrombin. The solution was then filtered through a 0.2-μm filter, placed in aliquots of 250 μL each, and stored at -80°C until use.

All animals were euthanized at the predetermined time point via intraperitoneal injections of ketamine and xylazine, followed by laparotomy, aortic rupture, and exsanguination.

In vitro release of cisplatin from the MFHH

To assess the rate of cisplatin release, 5.0 mg of MFHH was placed in 10 ml of phosphate-buffered saline (PBS, 0.01 M, pH 7.4). Additionally, 5.0 mg of MFHH was placed in 10 ml of phosphate-buffered saline (PBS, 0.01 M, pH 6.5). Both solutions were left at 37°C for 96 h. The concentration of cisplatin in the solutions was determined at regular intervals with a Zeeman Z-8000 atomic absorption spectrophotometer (Hitachi, Ltd., Tokyo, Japan).

Tumor volume determination

After constructing the subcutaneous Ehrlich tumor mouse model, the tumor volume was measured at autopsy after sampling for histopathological analysis at various time points. Tumor volume was calculated using the formula: volume = length × width × height × (π/6).

Cytological and histological examination

Cytological evaluation: Slides with imprints of tumor tissue were fixed with 95% ethanol, and stained by the Papanicolaou method. The cytological features of tumor tissue samples were assessed based on the shape of the nuclei, the increase in nucleoli, the density of the nucleus and necrotic background at various times after modeling and at the initiation of the treatment.

For histopathological examination, tumor tissues, together with the surrounding tissues, were fixed with 10% neutral buffered formalin, embedded in paraffin, and cut into 5-μm thick sections. Sections were stained with H&E, 6-diamidino-2-phenylindole (DAPI), and Masson's trichrome, according to the manufacturer's protocol. Cells were then immunostained with anti-Ki67 (incubation time, 20 min; clone MM1; dilution, 1:200; cat. no. PA0118; Leica Biosystems Newcastle Ltd.), and BSL-2 (incubation time, 20 min; Clone bcl-2/100/D5; dilution 1:100 for 30 min at 25°C; Leica Biosystems Newcastle Ltd.), anti-cytokeratin 19 (RCK108; ab9221; dilution 1:200) antibodies using the Novolink DAB Polymer Detection system (incubation time, 20 min; cat no. RE7260-CE; Leica Biosystems Newcastle Ltd.), according to the manufacturer's protocol. Endogenous peroxidase activity was neutralized using a Peroxidase Block reagent (3-4% [v/v] hydrogen peroxide; Novolink DAB Polymer Detection system; cat. no. RE7260-CE; Leica Biosystems Newcastle Ltd.). Subsequently, the cells were incubated with the rabbit anti-mouse IgG (<10 μg/mL) antibodies in 10% (v/v) animal serum in Tris-buffered saline/0.1% ProClin 950 (Novolink DAB Polymer Detection system). All immunohistochemical reactions were performed at room temperature. Images were acquired using a Leica DMLB microscope (Leica Application Suite v.3.6.0; Wetzlar, Germany).

Scanning electron microscopy

Collected tumor tissues and cisplatin gel together with the surrounding tissues were immersed in a fixative solution containing 2.5% glutaraldehyde and 4% paraformaldehyde in 0.1 M phosphate buffer. After fixation, the samples were dehydrated with various concentrations of ethanol, immersed in a mixture of 95% ethanol and isoamyl acetate (1:1) for 10 min, and in pure isoamyl acetate for 15 min. After removing isoamyl acetate, the samples were dried using a Tousimis Samdri-780 critical-point dryer (Tousimis Research Corporation). Then, the tissues were sputter-coated with gold and visualized using a JEOL JSM-65 10 LW scanning electron microscope (JEOL, Ltd.).

Energy dispersive spectroscopy

Energy dispersive spectroscopy was used to determine the amount of Pt nanoparticles in the gel before and after application to the wound. Analytical AztecEnergy-EDS software (Oxford Instruments, Inc.) and X-MaxN SDD detector (Oxford Instruments, Inc.) were used for the energy dispersive analysis of scanning electron microscopy results.

Statistical analysis

GraphPad Prism 9.0 (GraphPad Software, Inc.) was used to process statistical data. At each time point, the destruction of tumor cells was assessed and compared between groups. Tukey's post-hoc tests and one-way analysis of variance were used to compare differences between several groups. $P<0.05$ was considered to indicate a statistically significant difference.

Results

In vitro studies showed that MFHH that was placed in PBS (pH 6.5) at 37°C degraded faster during the first two days than MFHH placed in PBS (pH 7.4). **Figure 1** showing the in vitro degradation profiles of MFHH, demonstrates that a burst of MFHH degradation occurs in the first hours after being placed in PBS solutions. Afterwards, the degradation of MFHH in solutions slightly decreased and continued to decrease in the following hours. If we consider the fact that the pH values in normal tissues are in the range of 7.2-7.5, and the pH of tumor cells is in the range of 6.4-7.0 [41], then we can conclude that the pH of the tumor tissue can enhance the degradation of MFHH. **Figure 2** also shows the rate of tumor growth in all groups of animals.

In our study, a solid oval-shaped tumor with a volume of 200 ± 8 mm^3 was detected in the skin of all animals 20 days after inoculation. The color of the fur and skin around the tumor remained unchanged.

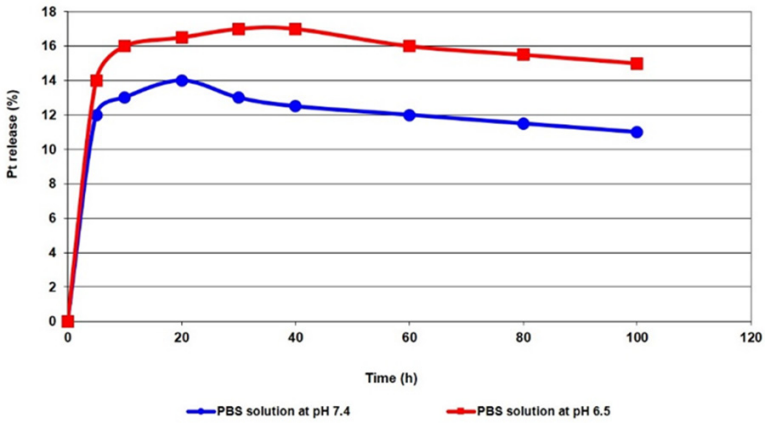

Figure 1. In vitro degradation profiles of MFHH.

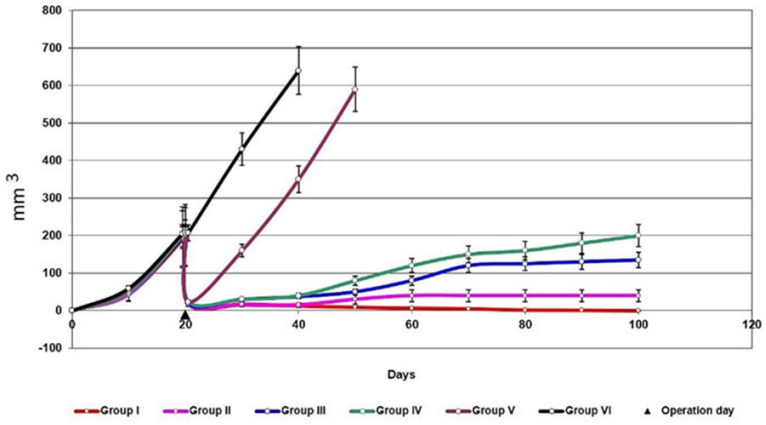

Figure 2. Tumor growth rate in all groups of animals.

Group	Treatment Methods	The degree of destruction of cancer cells				
		I	II a	II b	III	IV
I	TM+TR+ MFHH	-	-	-	-	+
II	TM+TR+ GHC	-	-	-	+	-
III	TM+TR+ CS-BMSCs	-	-	+	-	-
IV	TM+ TR + iv BMSCs	-	+	-	-	-
V	TM + TR	+	-	-	-	-
VI	TM	+	-	-	-	-

Figure 3. Histopathological response to treatment according to the Evans classification scheme. Degree I (<10%) of destruction of cancer cells or its complete absence; IIa degree, destruction of 10-50% of cancer cells; IIb degree, destruction of 51-90% of cancer cells; Grade III, few (<10%) viable cancer cells are present; Grade IV, viable cancer cells are completely absent. (TM) - tumor model, (TR) - resection of 90% of the tumor, (MFHH) - multifunctional hybrid hydrogel, (GHC) - gelatin hydrogels incorporating cisplatin, (CS-BMSCs) - CultiSpher loaded with BMSCs.

In animals of the fifth group, 6-8 days after tumor resection, the sutures were opened, and residual tumor tissue and purulent exudate were observed in the wound. Within a week, the residual tumor had no signs of progression. However, on days 10-12, a sharp increase in tumor growth was observed, and the wound itself took on a chronic course. The histopathological response to each treatment was determined (**Figure 3**) according to the Evans classification scheme [42, 43]. The percentage of destructed cancer cells was calculated and compared between groups over the experimental period. ****P< 0.0001; Statistically significant difference between groups using one-way ANOVA, post-hoc Tukey test. Two weeks after tumor resection, histopathological studies of animals of the fifth group (**Figure 4**) have revealed the presence of tumor cells with cytoplasmic vacuolization and signs of karyolysis along the periphery of the residual tumor. Inflammatory lymphocytic infiltration around the residual tumor was mild. Tumor cells with anaplastic characteristics and nuclear pleomorphism were observed in the central part of the residual tumor. Several mitotic cells have also been identified. DAPI staining has revealed an increased luminescence in the nuclei of tumor cells. Tumor cells penetrated the muscles 20 days from the resection. A similar histopathological observation was found in animals of the sixth group, in which the animals did not receive any treatment. Immunohistochemical studi-

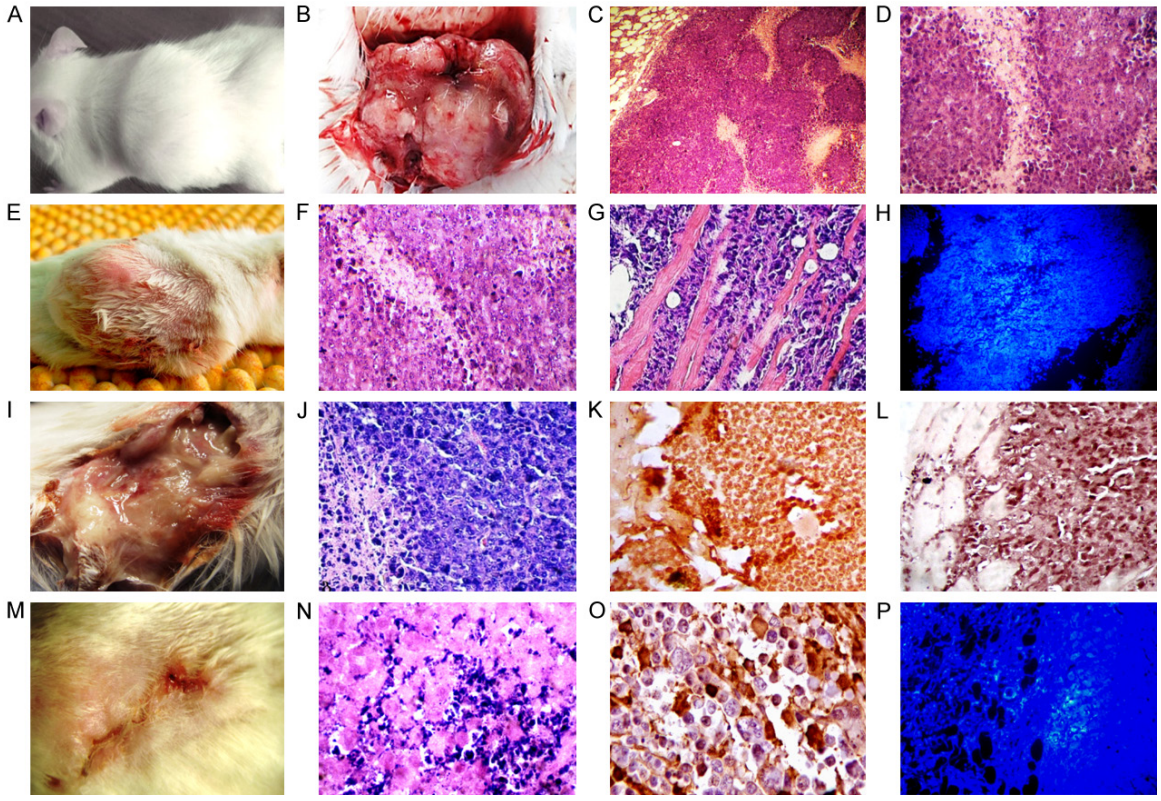

Figure 4. Ehrlich subcutaneous tumor model before and after the treatment with gelatin hydrogels incorporating cisplatin (GHC). A. Ehrlich subcutaneous tumor model. Observation period is 20 days; B. Gross section of subcutaneous Ehrlich tumor; C, D. Structural heterogeneity of the tumor, where viable areas are interspersed with necrotic zones. The well-defined tumor capsule, mainly composed by connective tissue. H&E staining, X200, 400; E. The animals of group VI with a tumor model without treatment. Observation period is 20 days; F, G. Anaplastic cells with anarchic progression, and invasion of tumor cells into muscle tissue. H&E staining, X400; H. Staining for DAPI revealed enhanced luminescence in the nuclei of tumor cells. X200; I. The wound suture failure. Observation period is 5 days; J. Layers of tumor cells with necrotic and hemorrhagic areas. H&E staining, X400; K, L. Immunohistochemical studies revealed a high level of expression of Ki-67 and BCL-2 markers; M. In most GHC-treated animals, the wound healed without complications. Observation period is 45 days; N. Destruction of 50% of cancer cells after GHC treatment. H&E staining, X400. Observation period is 30 days; O. Immunohistochemical studies revealed a low level of expression of Ki-67 markers; P. Staining for DAPI revealed a slight increase in luminescence in the nuclei of tumor cells. X200.

es revealed high expression levels of Ki-67 and Bcl-2. All animals of the 5th and 6th groups have died within 1.5-2 months of observation, mainly due to tumor progression.

All animals in the first group survived and were observed for five months after treatment. The wound healed without any complications. Locoregional recurrence and distant metastases were not observed. Histopathological studies (**Figure 5**) revealed that MFHH treated animals exhibited extensive areas of necrosis, edema, and destructive changes in the tumor tissue along the periphery of the residual tumor. Most tumor cells showed karyorrhexis and karyolysis due to the damaging effects of MFHH. Along the edge of the necrotic zone of the residual tumor, inflammatory leukocyte infiltration was visible, which may be associated with a strong immune response. Notably, DAPI staining of residual tumor fragments revealed a significant decrease in the number of tumor cell nuclei after MFHH treatment. After 20 d, no luminescence was detected in the tumor cell nuclei. H&E and Masson's trichrome staining revealed the formation of connective tissues with new vessels around the CultiSpher during the first week. One-month later, well-formed tissues were observed around the CultiSpher, which started undergoing resorption. Masson's trichrome staining revealed the presence of collagen fibers around the CultiSpher. Immuno-

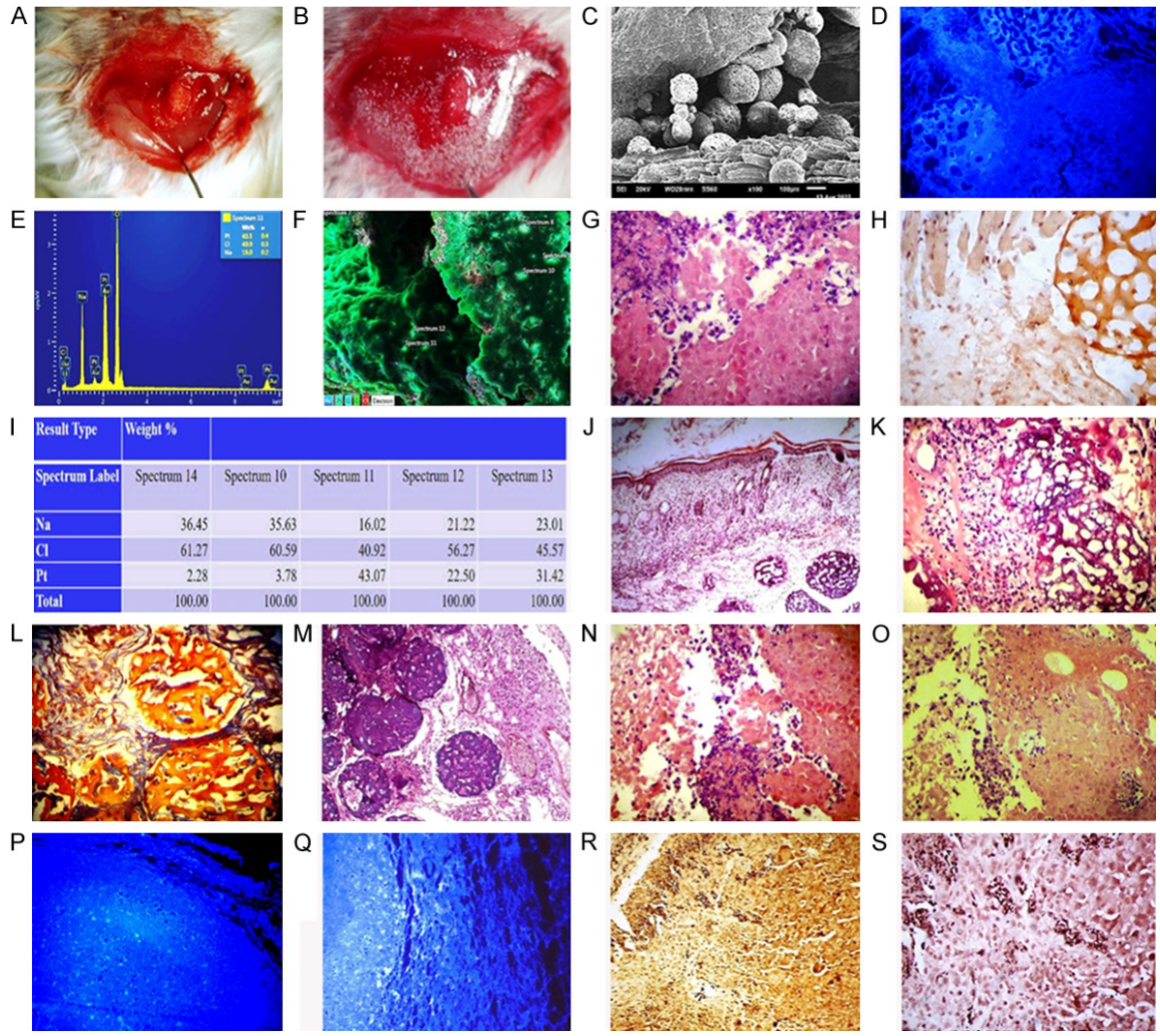

Result Type	Weight %				
Spectrum Label	Spectrum 14	Spectrum 10	Spectrum 11	Spectrum 12	Spectrum 13
Na	36.45	35.63	16.02	21.22	23.01
Cl	61.27	60.59	40.92	56.27	45.57
Pt	2.28	3.78	43.07	22.50	31.42
Total	100.00	100.00	100.00	100.00	100.00

Figure 5. Subcutaneous Ehrlich tumor after MFHH and BMSCs treatment. A. Residual tumor after the removal of 90% of the tumor mass; B. The wound is covered with MFHH; C. Scanning electron microscopy confirmed the diffuse distribution of CultiSpher in the wound; D. Staining for DAPI revealed no luminescence. X200; E, F. The platinum nanoparticles are evenly distributed both on the surface of the MFHH and inside the tumor cells; G. Cancer cells destruction after MFHH treatment. H&E staining, X400. Observation period is 30 days; H. Immunohistochemical studies revealed a low level of expression of Ki-67 markers. X200; I. MFHH contains 40 wt% of platinum nanoparticles in different spectra; J. The wound healed without complications after MFHH treatment. H&E staining, X200. Observation period is 30 days; K. The process of resorption of Cultispheres. H&E staining, X800. Observation period is 40 days; L. Collagen fibers around CultiSpheres. Masson's trichrome stain, X800; M. Connective tissue with new vessels around the CultiSpher. H&E staining, X800; N. After the injection of Cultispheres loaded with BMSCs into the wound, >50% of the cancer cells were destroyed. H&E staining, X800. Observation period is 30 days; O. After iv injection of BMSCs, <50% of the cancer cells were destroyed. H&E staining, X800. Observation period is 30 days; P, Q. Staining for DAPI showed weak luminescence of tumor cell nuclei. X200; R, S. Immunohistochemical studies revealed a low level of expression of Ki-67 and BCL-2 markers. X200.

histochemical studies revealed low expression levels of Ki-67 markers. Scanning electron microscopy confirmed the diffuse distribution of CultiSpher in the wound. On the 20-25th day, wound healing was observed without complications. It should be noted, that the CultiSphers were gradually subjected to resorption.

In animals of the second group, >50% of cancer cells were destroyed within a month from the initiation of treatment. In the tissue of the residual tumor, numerous necrotic wounds were detected both in the center and along the periphery of the tumor. Notably, DAPI staining of residual tumor fragments revealed a signifi-

cant decrease in the number of tumor cell nuclei. Immunohistochemical studies revealed a low level expression of Ki-67 markers. Out of ten animals of this group, three (30%) have died. In two dead animals, the failure of the wound sutures with abundant purulent exudate has developed on the 5th-7th day. Another animal of this group has died due to unknown reasons on the 28th day from the initiation of the treatment. At the same time, after the introduction of CS-BMSCs, destruction of <50% of cancer cells was observed in the remaining tumor tissue. Extensive areas of necrosis, edema and destructive changes in the tumor tissue were detected. Mainly, these changes were observed along the periphery of the residual tumor. Karyorrhexis and karyolysis of most of the tumor cells were detected in the central part. A similar picture was observed in animals of the fourth group after a single intravenous injection of BMSCs. Histopathological studies revealed the presence of tumor cells with cytoplasmic vacuolization and signs of karyolysis. There was a strong inflammatory lymphocytic infiltration around the residual tumor. Immunohistochemical studies revealed low expression levels of Ki-67 and Bcl-2. It should be noted that intravenous administration of BMSCs and administration of Cultispheres loaded with BMSCs into the tumor bed promoted inhibition of residual tumor growth, which was confirmed by residual tumor volume calculation with histopathological methods, and animal survival. However, the survival of animals after the injection of Cultispheres loaded with BMSCs in the tumor bed was higher (60% survivors) compared to animals who received an intravenous injection of BMSCs (30% survivors). We associated this to the direct effect of CS-BMSCs on both the remaining tumor tissue and surrounding tissues.

Discussion

MFHH that was developed in this study is useful for the local delivery of cisplatin to tumors, with excellent anti-cancer efficacy and minimal side effects. Notably, MFHH is easy to manufacture and does not require expensive reagents, complex protocols, or specialized equipment. Component A of MFHH, which consists of a cross-linked hydrogel, can be obtained by simply mixing gelatin with cisplatin. Similarly, the gel used for component B can be easily formed by mixing fibrinogen and thrombin. Allogeneic freeze-dried stem cells used to load CultiSpher can be obtained from various sources, including bone marrow, adipose tissue, human placenta, and umbilical cord blood. CultiSpher loaded with stem cells can be stored at the room temperature for long periods before use. Both components of MFHH can be injected into a wound using conventional syringes. Here, MFHH did not aggregate or block the 20 or 22 gauge needles and completely covered the bottom of the wound along with the residual tumor, enveloping it from all sides with a gradual release of platinum cisplatin nanoparticles. Nanoparticles with an optimal size of 80-160 nm preferentially enter tumors because of the enhanced permeability and retention (EPR) effect [44]. We hypothesized that MFHH, owing to the EPR effect, can carry out intratumoral delivery of the required amount of cisplatin to effectively eliminate the tumor cells with limited side effects. Cisplatin entering the tumor cell via passive diffusion or endocytosis kills the cancer cells by damaging their DNA, mainly by forming Pt-d (GpG) and, to a lesser extent, Pt-d (ApG) and Pt-d (GpXpG) intrastrand diadducts and Pt-G-G interstrand cross-links at low frequencies [45]. Scanning electron microscopy revealed that the platinum nanoparticles were evenly distributed on both the MFHH surface and inside the tumor cells. Energy dispersive spectroscopy revealed that MFHH contained 40-43 wt% platinum nanoparticles in various spectra. After being placed into the wound, the amount of platinum nanoparticles in the spectra did not change for three months, indicating their gradual long-term effect on residual tumor cells. Moreover, cancer cell death and tumor regression contributed to wound healing without any complications. Wound healing is a dynamic process that involves highly organized cellular, humoral, and molecular mechanisms. It consists of overlapping steps, such as hemostasis, inflammation, proliferation, and maturation (remodeling). At each stage, the wound microenvironment and various cells, including fibroblasts, leukocytes, neutrophils, macrophages, and lymphocytes, play active roles in the wound healing process. Molecular mechanisms of wound healing have been described in previous studies [46]. Disturbance at any stage in the residual tumor tissue can cause chronic inflammation, further contributing to tumor progression [47].

In most animals in the second group, the sutures failed in the presence of abundant purulent exudate two weeks after the resection of 90% of tumor mass. Of course, the reader may wonder why we did not remove 100% of the tumor mass as in the clinical setting. We made it harder for ourselves because we assumed that MFHH could be used for inoperable cancer. Our next study will focus on this issue.

Histopathological studies of the residual tumor in the animals of the second group revealed the presence of a distinct capsule of connective tissue infiltrated with polymorphonuclear lymphocytes and tumor cells around the residual tumor. Necrotic areas with inflammatory cells and many mitotic and anaplastic cells were observed in the tumor tissues. All animals in this group died from suture failure, chronic inflammation, and tumor progression within a month of surgery.

We have demonstrated that, treatment with MFHH led to complete wound healing without any complications, which was facilitated by the both components of MFHH. Component A actively eliminated the residual cancer cells, and component B, containing CultiSpher loaded with freeze-dried BMSCs accelerated the wound healing process. Scanning electron microscopy revealed that CultiSpher has a porous structure, and the attached cells can grow on its inner and outer surfaces. These results indicate that both cisplatin and freeze-dried BMSCs, especially their paracrine factors, play key roles in wound healing.

Over the years, use of BMSCs for the treatment of non-healing wounds has gained increasing attention. After direct injection into a wound, MSCs can regulate the wound healing process via early activation of matrix metalloproteinase-9 and vascular endothelial growth factor [48, 49]. In addition, MSCs can support tissue regeneration in the proliferation phase and promote the production of extracellular matrix [50, 51]. An animal experiment revealed that systemic administration of allogeneic and syngeneic BMSCs causes rapid resolution of the acute inflammatory phase and early formation of granulation tissue, facilitating wound healing [52].

Effects of MSCs on tumor pathogenesis are controversial [53]. Some authors suggest that, MSCs promote tumor proliferation and metastasis [54, 55]. On the contrary, others report that human mesenchymal stem cells exert potent antitumorigenic effects in a model of Kaposi's sarcoma [56]. The authors have demonstrated the molecular mechanism of inhibitory effect of human mesenchymal stem cells (hMSCs) on the growth of human MCF-7 breast cancer cells [57]. It is also reported that in large numbers, MSCs are potentially cytotoxic and when injected locally in the tumor tissue they might be effective antiangiogenesis agents suitable for cancer therapy [58]. There are reports that downregulation of X-linked inhibitor of apoptosis protein (XIAP) with human umbilical cord blood mesenchymal stem cell (hUCBSC) treatment has induced apoptosis, which led to the death of the glioma cells and xenograft cells [59]. An experimental study has demonstrated that MSCs had potential inhibitory effects on tumor cell growth in vitro and in vivo without host immunosuppression by inducing apoptotic cell death and G (0)/G (1) phase arrest of cancer cells [60].

As we noted above, paracrine signals of mesenchymal stem cells are associated with immunomodulatory properties, angiogenesis, anti-inflammatory action, cell proliferation, and others. At the same time, MSCs to have antitumor activity, and one of the mechanisms by which they exert this effect is through paracrine signaling [61]. For example, the paracrine effects of mesenchymal stem cells induce aging and differentiation of glioblastoma stem cells [62]. MSC-derived exosomes may serve as a significant mediator of cell-to-cell communication within the tumor microenvironment and suppress angiogenesis by transferring anti-angiogenic molecules [63]. MSC-derived exosomes also inhibit prostate cancer cell migration and invasion by Down-Regulating Trefoil Factor 3 (TFF3) [64].

Others, on the contrary, believe that MSCs are able to secrete angiogenic factors (FGF-2, PDGF, VEGF, TGF-β, IL-6, IL-8, and angiopoietin-1) that promote angiogenesis and tumor development. In addition, the direct effect of MSC paracrine factors on immune cells inhibits apoptosis or suppresses T cell proliferation,

which leads to a decrease in immunogenic activity [61, 65].

Thus, we can conclude that the question of the role of paracrine factors in stimulating growth or inhibiting tumor cells remains open to date.

We decided to explore the possibility of using paracrine factors of lyophilized MSCs to suppress tumor growth. Why freeze-dried MSCs? Freeze-drying or lyophilization is a process of removing water from a biological material, such as stem cells, to create a dry and stable product that can be stored for long periods at room temperature. The authors have noted that after lyophilization, the MSCs retain more than 80% of paracrine factors [66]. Lyophilization also provides a number of advantages over traditional stem cell therapy, including ease of storage, transport, and administration, as well as lower costs and less risk of infection. Our studies have shown that after the injection of CultiSpher loaded with BMSCs, <50% of cancer cells were destroyed in the remaining tumor tissue. Immunohistochemical studies have revealed low expression levels of Ki-67 and Bcl-2. It should be mentioned that intravenous administration of BMSCs and administration of Cultispheres loaded with BMSCs to the tumor bed has contributed to the inhibition of residual tumor growth, which was confirmed by residual tumor volume calculation with histopathological methods. However, the survival rate of animals that received an injection of Cultispheres loaded with BMSCs into the tumor bed was higher compared to animals that received intravenous injection of BMSCs. We associated this to the direct effect of BMSCs on both tumor cells and surrounding tissues.

In preclinical studies, freeze-dried MSCs have shown promise in the treatment of various pathologies. For example, the authors demonstrated the possibility of using freeze-drying strategy to store human bone marrow mesenchymal stem/stromal derived extracellular vesicles for applications in stroke [67]. Our previous study has also shown the effectiveness of dried stem cells for the treatment of nonhealing wound after radiation therapy [68]. While the results of preclinical studies are promising, more research is needed to determine the safety and efficacy of freeze-dried stem cells. Additionally, regulatory agencies such as the FDA has not yet approved the use of freeze-dried stem cells for clinical use.

Conclusion

In this study, we fabricated MFHH for the direct local delivery of cisplatin to tumor cells and demonstrated its excellent anti-cancer efficacy with minimal side effects. MFHH gradually released the required amount of cisplatin to destroy the residual tumor, thereby preventing loco-regional tumor recurrence. We have also demonstrated that BMSCs are able to inhibit residual tumor growth. Moreover, CultiSpher built a three-dimensional structure in the wound and the paracrine factors of freeze-dried BMSCs accelerated the wound healing process. The components of the MFHH can be used both separately and together. However, for the successful application of MFHH in clinical practice, it is necessary to study in more detail the role of paracrine factors of freeze-dried BMSCs in the inhibition or proliferation of residual cancer. These questions will be the focus of our future research.

Disclosure of conflict of interest

None.

Address correspondence to: Dr. Teona Paresishvili, Department of Clinical Anatomy, Tbilisi State Medical University, 33 Vazha-Pshavela Avenue, Tbilisi 0186, Georgia. E-mail: t.paresishvili@tsmu.edu

References

[1] Pierik AS, Leemans CR and Brakenhoff RH. Resection margins in head and neck cancer surgery: an update of residual disease and field cancerization. Cancers (Basel) 2021; 13: 26-35.

[2] Endo M and Lin PP. Surgical margins in the management of extremity soft tissue sarcoma. Chin Clin Oncol 2018; 7: 37.

[3] Maloney BW, McClatchy DM, Pogue BW, Paulsen KD, Wells WA and Barth RJ. Review of methods for intraoperative margin detection for breast conserving surgery. J Biomed Opt 2018; 23: 1-19.

[4] Graeser M, Schrading S, Gluz O, Strobel K, Herzog C, Umutlu L, Frydrychowicz A, Rjosk-Dendorfer D, Würstlein R, Culemann R, Eulenburg C, Adams J, Nitzsche H, Prange A, Kümmel S, Grischke EM, Forstbauer H, Braun M, Poten-

berg J, von Schumann R, Aktas B, Kolberg-Liedtke C, Harbeck N, Kuhl CK and Nitz U. Magnetic resonance imaging and ultrasound for prediction of residual tumor size in early breast cancer within the ADAPT subtrials. Breast Cancer Res 2021; 23: 36.

[5] Eo JS, Paeng JC and Lee DS. Nuclear imaging for functional evaluation and theragnosis in liver malignancy and transplantation. World J Gastroenterol 2014; 20: 5375-88.

[6] Tang R, Saksena M, Coopey SB, Fernandez L, Buckley JM, Lei L, Aftreth O, Koerner F, Michaelson J, Rafferty E, Brachtel E and Smith BL. Intraoperative micro-computed tomography (micro-CT): a novel method for determination of primary tumour dimensions in breast cancer specimens. Br J Radiol 2016; 89: 20150581.

[7] Gallamini A, Zwarthoed C and Borra A. Positron emission tomography (PET) in oncology. Cancers (Basel) 2014; 6: 1821-89.

[8] Holt D, Parthasarathy AB, Okusanya O, Keating J, Venegas O, Deshpande C, Karakousis G, Madajewski B, Durham A, Nie S, Yodh AG and Singhal S. Intraoperative near-infrared fluorescence imaging and spectroscopy identifies residual tumor cells in wounds. J Biomed Opt 2015; 20: 76002.

[9] D'Amato Figueiredo MV, Alexiou GA, Vartholomatos G and Rehder R. Advances in intraoperative flow cytometry. Int J Mol Sci 2022; 23: 13430.

[10] De Bonis P, Anile C, Pompucci A, Fiorentino A, Balducci M, Chiesa S, Lauriola L, Maira G and Mangiola A. The influence of surgery on recurrence pattern of glioblastoma. Clin Neurol Neurosurg 2013; 115: 37-43.

[11] Sperti C, Pasquali C, Piccoli A and Pedrazzoli S. Recurrence after resection for ductal adenocarcinoma of the pancreas. World J Surg 1997; 21: 195-200.

[12] Zhang Y, Frampton AE, Kyriakides C, Bong JJ, Habib N, Ahmad R and Jiao LR. Loco-recurrence after resection for ductal adenocarcinoma of the pancreas: predictors and implications for adjuvant chemoradiotherapy. J Cancer Res Clin Oncol 2012; 138: 1063-71.

[13] Mashiko T, Ogasawara T, Masuoka Y, Ei S, Takahashi S, Mori M, Koyanagi K, Yamamoto S and Nakagohri T. Indications for resection of recurrent lesions in patients with distal cholangiocarcinoma based on prognostic factors: a single-institute retrospective study and brief literature review. BMC Surg 2022; 22: 423.

[14] Okusaka T. Treatment for postoperative recurrence of pancreatic cancer: a narrative review. Chin Clin Oncol 2022; 11: 19.

[15] Liska D, Stocchi L, Karagkounis G, Elagili F, Dietz DW, Kalady MF, Kessler H, Remzi FH and Church J. Incidence, patterns, and predictors of locoregional recurrence in colon cancer. Ann Surg Oncol 2017; 24: 1093-1099.

[16] Aderson K and Hamm RL. Factors that impair wound healing. J Am Coll Clin Wound Spec 2012; 4: 84-91.

[17] Kumar S, Juresic E, Barton M and Shafiq J. Management of skin toxicity during radiation therapy: a review of the evidence. J Med Imag Radiat Oncol 2010; 54: 264-79.

[18] Mendonça JJ and Juiz-Lopez P. Regenerative facial reconstruction of terminal stage osteoradionecrosis and other advanced craniofacial diseases with adult cultured stem and progenitor cells. Plast Reconstr Surg 2010; 126: 1699-709.

[19] Deptuła M, Zieliński J, Wardowska A and Pikuła M. Wound healing complications in oncological patients: perspectives for cellular therapy. Postepy Dermatol Alergol 2019; 36: 139-146.

[20] Harless WW. Revisiting perioperative chemotherapy: the critical importance of targeting residual cancer prior to wound healing. BMC Cancer 2009; 9: 118.

[21] Burris HA 3rd, Vogel CL, Castro D, Mishra L, Schwarz M, Spencer S, Oakes DD, Korey A and Orenberg EK. Intratumoral cisplatin/epinephrine-injectable gel as a palliative treatment for accessible solid tumors: a multicenter pilot study. Otolaryngol Head Neck Surg 1998; 118: 496-503.

[22] Malhotra H and Plosker GL. Cisplatin/epinephrine injectable gel. Drugs Aging 2001; 18: 787-93.

[23] Leung TW, Yu S, Johnson PJ, Geschwind J, Vogl TJ, Engelmann K, Gores GJ, Giovannini M, O'Grady J, Heneghan M, Stewart M, Orenberg EK and Thuluvath PJ. Phase II study of the efficacy and safety of cisplatin-epinephrine injectable gel administered to patients with unresectable hepatocellular carcinoma. J Clin Oncol 2003; 21: 652-8.

[24] Kerr C. Cisplatin gel treatment of unresectable liver cancer. Lancet Oncol 2003; 4: 199.

[25] Qian K, Qian H, Cai J, Yue W, Yu X and Liu B. Evaluation of cisplatin-hydrogel for improving localized antitumor efficacy in gastric cancer. Pathol Res Pract 2019; 215: 755-760.

[26] Yildirim M, Weiss AV and Schneider M. The effect of elasticity of gelatin nanoparticles on the interaction with macrophages. Pharmaceutics 2023; 15: 199.

[27] Han S, Li M, Liu X, Gao H and Wu Y. Construction of amphiphilic copolymer nanoparticles based on gelatin as drug carriers for doxorubicin delivery. Colloids Surf B Biointerfaces 2013; 102: 833-41.

[28] Abdelrady H, Hathout RM, Osman R, Saleem I and Mortada ND. Exploiting gelatin nanocarri-

ers in the pulmonary delivery of methotrexate for lung cancer therapy. Eur J Pharm Sci 2019; 133: 115-126.
[29] Zhou K, Zhu Y, Chen X, Li L and Xu W. Redox- and MMP-2-sensitive drug delivery nanoparticles based on gelatin and albumin for tumor targeted delivery of paclitaxel. Mater Sci Eng C Mater Biol Appl 2020; 114: 111006.
[30] Fan Y, Yuan S, Huo M, Chaudhuri AS, Zhao M, Wu Z and Qi X. Spatial controlled multistage nanocarriers through hybridization of dendrimers and gelatin nanoparticles for deep penetration and therapy into tumor tissue. Nanomedicine 2017; 13: 1399-1410.
[31] Andronescu E, Ficai A, Albu MG, Mitran V, Sonmez M, Ficai D, Ion R and Cimpean A. Collagen-hydroxyapatite/cisplatin drug delivery systems for locoregional treatment of bone cancer. Technol Cancer Res Treat 2013; 12: 275-84.
[32] Hong SH, Li Y, Eom JB and Choi Y. Responsive alginate-cisplatin nanogels for selective imaging and combined chemo/radio therapy of proliferating macrophages. Quant Imaging Med Surg 2018; 8: 733-742.
[33] Yu T, Li Y, Gu X and Li Q. Development of a hyaluronic acid-based nanocarrier incorporating doxorubicin and cisplatin as a pH-sensitive and CD44-targeted anti-breast cancer drug delivery system. Front Pharmacol 2020; 11: 532457.
[34] Shen X, Wang Y, Xi L, Su F and Li S. Biocompatibility and paclitaxel/cisplatin dual loading of nanotubes prepared from poly (ethylene glycol)-polylactide-poly (ethylene glycol) triblock copolymers for combination cancer therapy. Saudi Pharm J 2019; 27: 1025-1035.
[35] Khiati S, Luvino D, Oumzil K, Chauffert B, Camplo M and Barthélémy P. Nucleoside-lipid-based nanoparticles for cisplatin delivery. ACS Nano 2011; 5: 8649-55.
[36] Senapati S, Mahanta AK, Kumar S and Maiti P. Controlled drug delivery vehicles for cancer treatment and their performance. Signal Transduct Target Ther 2018; 16: 3-7.
[37] Suzuki T, Tsunoda S, Yamashita K, Kuwahara T, Ando M, Tabata Y and Obama K. A simple preparation method of gelatin hydrogels incorporating cisplatin for sustained release. Pharmaceutics 2022; 14: 2601.
[38] O'Connell CD, Onofrillo C, Duchi S, Li X, Zhang Y, Tian P, Lu L, Trengove A, Quigley A, Gambhir S, Khansari A, Mladenovska T, O'Connor A, Di Bella C, Choong PF and Wallace GG. Evaluation of sterilisation methods for bio-ink components: gelatin, gelatin methacryloyl, hyaluronic acid and hyaluronic acid methacryloyl. Biofabrication 2019; 11: 035003.
[39] Kakabadze MZ, Paresishvili T, Mardaleishvili K, Vadachkoria Z, Kipshidze N, Jangavadze M, Karalashvili L, Ghambashidze K, Chakhunashvili D and Kakabadze Z. Local drug delivery system for the treatment of tongue squamous cell carcinoma in rats. Oncol Lett 2022; 23: 13.
[40] Yuan Ye K, Sullivan KE and Black LD. Encapsulation of cardiomyocytes in a fibrin hydrogel for cardiac tissue engineering. J Vis Exp 2011; 55: 3251.
[41] Hao G, Xu ZP and Li L. Manipulating extracellular tumour pH: an effective target for cancer therapy. RSC Adv 2018; 8: 22182-22192.
[42] Evans DB, Rich TA, Byrd DR, Cleary KR, Connelly JH, Levin B, Charnsangavej C, Fenoglio CJ and Ames FC. Preoperative chemoradiation and pancreaticoduodenectomy for adenocarcinoma of the pancreas. Arch Surg 1992; 127: 1335-9.
[43] Hiroshima Y, Zhao M, Zhang Y, Zhang N, Maawy A, Murakami T, Mii S, Uehara F, Yamamoto M, Miwa S, Yano S, Momiyama M, Mori R, Matsuyama R, Chishima T, Tanaka K, Ichikawa Y, Bouvet M, Endo I and Hoffman RM. Tumor-targeting salmonella typhimurium A1-R arrests a chemo-resistant patient soft-tissue sarcoma in nude mice. PLoS One 2015; 10: e0134324.
[44] Wu J. The enhanced permeability and retention (EPR) effect: the significance of the concept and methods to enhance its application. J Pers Med 2021; 11: 771.
[45] Rennick JJ, Johnston APR and Parton RG. Key principles and methods for studying the endocytosis of biological and nanoparticle therapeutics. Nat Nanotechnol 2021; 16: 266-276.
[46] Foster DS, Jones RE, Ransom RC, Longaker MT and Norton JA. The evolving relationship of wound healing and tumor stroma. JCI Insight 2018; 3: e99911.
[47] Zhao H, Wu L, Yan G, Chen Y, Zhou M, Wu Y and Li Y. Inflammation and tumor progression: signaling pathways and targeted intervention. Signal Transduct Target Ther 2021; 6: 263.
[48] Brown JM, Nemeth K, Kushnir-Sukhov NM, Metcalfe DD and Mezey E. Bone marrow stromal cells inhibit mast cell function via a COX2-dependent mechanism. Clin Exp Allergy 2011; 41: 526-534.
[49] Jeon YK, Jang YH, Yoo DR, Kim SN, Lee SK and Nam MJ. Mesenchymal stem cells' interaction with skin: wound-healing effect on fibroblast cells and skin tissue. Wound Repair Regen 2010; 18: 655-61.
[50] Jin G, Prabhakaran MP and Ramakrishna S. Stem cell differentiation to epidermal lineages on electrospun nanofibrous substrates for skin tissue engineering. Acta Biomater 2011; 7: 3113-3122.
[51] Wu Y, Chen L, Scott PG and Tredget EE. Mesenchymal stem cells enhance wound healing

through differentiation and angiogenesis. Stem Cells 2007; 25: 2648-2659.
[52] McFarlin K, Gao X, Liu YB, Dulchavsky DS, Kwon D, Arbab AS, Bansal M, Li Y, Chopp M, Dulchavsky SA and Gautam SC. Bone marrow-derived mesenchymal stromal cells accelerate wound healing in the rat. Wound Repair Regen 2006; 14: 471-8.
[53] Klopp AH, Gupta A, Spaeth E, Andreeff M and Marini F. Concise review: dissecting a discrepancy in the literature: do mesenchymal stem cells support or suppress tumor growth? Stem Cells 2011; 29: 11-19.
[54] Chen J, Ji T, Wu D, Jiang S, Zhao J, Lin H and Cai X. Human mesenchymal stem cells promote tumor growth via MAPK pathway and metastasis by epithelial mesenchymal transition and integrin α5 in hepatocellular carcinoma. Cell Death Dis 2019; 10: 425.
[55] Ahn SY. The role of MSCs in the tumor microenvironment and tumor progression. Anticancer Res 2020; 40: 3039-3047.
[56] Khakoo AY, Pati S, Anderson SA, Reid W, Elshal MF, Rovira II, Nguyen AT, Malide D, Combs CA, Hall G, Zhang J, Raffeld M, Rogers TB, Stetler-Stevenson W, Frank JA, Reitz M and Finkel T. Human mesenchymal stem cells exert potent antitumorigenic effects in a model of Kaposi's sarcoma. J Exp Med 2006; 203: 1235-47.
[57] Qiao L, Xu ZL, Zhao TJ, Ye LH and Zhang XD. Dkk-1 secreted by mesenchymal stem cells inhibits growth of breast cancer cells via depression of Wnt signalling. Cancer Lett 2008; 269: 67-77.
[58] Otsu K, Das S, Houser SD, Quadri SK, Bhattacharya S and Bhattacharya J. Concentration-dependent inhibition of angiogenesis by mesenchymal stem cells. Blood 2009; 113: 4197-205.
[59] Dasari VR, Velpula KK, Kaur K, Fassett D, Klopfenstein JD, Dinh DH, Gujrati M and Rao JS. Cord blood stem cell-mediated induction of apoptosis in glioma downregulates X-linked inhibitor of apoptosis protein (XIAP). PLoS One 2010; 5: e11813.
[60] Lu YR, Yuan Y, Wang XJ, Wei LL, Chen YN, Cong C, Li SF, Long D, Tan WD, Mao YQ, Zhang J, Li YP and Cheng JQ. The growth inhibitory effect of mesenchymal stem cells on tumor cells in vitro and in vivo. Cancer Biol Ther 2008; 7: 245-51.
[61] Aldoghachi AF, Chong ZX, Yeap SK, Cheong SK, Ho WY and Ong AHK. Stem cells for cancer therapy: translating the uncertainties and possibilities of stem cell properties into opportunities for effective cancer therapy. Int J Mol Sci 2023; 24: 1012.
[62] Kološa K, Motaln H, Herold-Mende C, Koršič M and Lah TT. Paracrine effects of mesenchymal stem cells induce senescence and differentiation of glioblastoma stem-like cells. Cell Transplant 2015; 24: 631-44.
[63] Lee JK, Park SR, Jung BK, Jeon YK, Lee YS, Kim MK, Kim YG, Jang JY and Kim CW. Exosomes derived from mesenchymal stem cells suppress angiogenesis by down-regulating VEGF expression in breast cancer cells. PLoS One 2013; 8: e84256.
[64] Che Y, Shi X, Shi Y, Jiang X, Ai Q, Shi Y, Gong F and Jiang W. Exosomes derived from miR-143-overexpressing MSCs inhibit cell migration and invasion in human prostate cancer by downregulating TFF3. Mol Ther Nucleic Acids 2019; 18: 232-244.
[65] Liang W, Chen X, Zhang S, Fang J, Chen M, Xu Y and Chen X. Mesenchymal stem cells as a double-edged sword in tumor growth: focusing on MSC-derived cytokines. Cell Mol Biol Lett 2021; 26: 3.
[66] Peng Y, Xuan M, Zou J, Liu H, Zhuo Z, Wan Y and Cheng B. Freeze-dried rat bone marrow mesenchymal stem cell paracrine factors: a simplified novel material for skin wound therapy. Tissue Eng Part A 2015; 21: 1036-1046.
[67] Dorus B. Development of a freeze-drying strategy to store human bone marrow mesenchymal stem/stromal derived extracellular vesicles for applications in stroke. 2023; [Master's degree in Biomedical Engineering, University of Ottawa]. https://ruor.uottawa.ca/bitstream/10393/44569/3/Dorus_Brian_2023_thesis.pdf.
[68] Kakabadze Z, Chakhunashvili D, Gogilashvili K, Ediberidze K, Chakhunashvili K, Kalandarishvili K and Karalashvili L. Bone marrow stem cell and decellularized human amniotic membrane for the treatment of nonhealing wound after radiation therapy. Exp Clin Transplant 2019; 17: 92-98.